

# Fano physics behind the N-resonance in graphene

R.O. Kuzian,<sup>1,2</sup> D.V. Efremov,<sup>3</sup> and E.E. Krasovskii<sup>1,4,5</sup>

<sup>1</sup>*Donostia International Physics Center (DIPC), Paseo Manuel de Lardizabal 4, San Sebastián/Donostia, 20018 Basque Country, Spain*

<sup>2</sup>*Institute for Problems of Materials Science Krzhizhanovskogo 3, 03180 Kiev, Ukraine*

<sup>3</sup>*Leibniz Institute for Solid State and Materials Research Dresden, Helmholtzstrasse 20, D-01069 Dresden, Germany*

<sup>4</sup>*Departamento de Polímeros y Materiales Avanzados: Física, Química y Tecnología, Universidad del País Vasco-Euskal Herriko Unibertsitatea, Donostia-San Sebastián, 20080 Basque Country, Spain*

<sup>5</sup>*IKERBASQUE, Basque Foundation for Science, 48013 Bilbao, Spain*  
(Dated: December 25, 2024)

Bound states and scattering resonances in the unoccupied continuum of a two-dimensional crystal predicted in [Phys.Rev. B **87**, 041405(R) (2013)] are considered within an exactly solvable model. A close connection of the observed resonances with those arising in the Fano theory is revealed. The resonance occurs when the lateral scattering couples the layer-perpendicular incident electron wave to a strictly bound state. The coupling strength determines the location of the pole in the scattering amplitude in the complex energy plane, which is analytically shown to lead to a characteristic Fano-lineshape of the energy dependence of the electron transmissivity through the crystal. The implications for the timing of the resonance scattering are discussed. The analytical results are illustrated by *ab initio* calculations for a graphene monolayer.

## I. INTRODUCTION

The interest in the electronic properties of low-dimensional systems has been growing in the last decades owing to the plethora of unique quantum phenomena impossible in the three-dimensional (3D) extended systems [1–3]. A striking example are the bound states and scattering resonances in the unoccupied continuum of two-dimensional (2D) crystals [4]. In an infinite 3D crystal bound states cannot exist at any energy, whereas in a stand-alone 2D layer the electrons below the vacuum level  $E_{\text{vac}}$  are bound to the layer and those above  $E_{\text{vac}}$  can escape to infinity. However, as was first shown in Ref. [4] in atomically thin layers solutions of the Schrödinger equation may exist above the vacuum level that are bound to the layer, thereafter referred to as N-states. Such solutions may occur both at complex and at real energies, the former giving rise to scattering resonances and the latter being true stationary states—a rare example of a bound state in continuum (BIC) [5]. In contrast to von Neumann and Wigner BIC [6–9] in a 1D continuum and to those arising from the interaction of Feshbach’s resonances in the scattering on a spherically symmetric potential [10–12], the N-states are extended along the crystal plane and bound in the perpendicular direction. In Ref. 4, scattering resonances related to complex-energy N-states were predicted to exist in graphene, where they were soon observed experimentally [13–22] and further studied theoretically [13, 23–27].

Conventional band structure or low energy electron diffraction (LEED) calculations are performed for real energies, so the parameters of the resonance cannot be directly inferred. This calls for the development of an analytical model that would provide a functional relation between the complex energy of the resonance and

the observables. In the original theory, the resonances appeared as a result of sophisticated analytical computations for a specific model or as an *ab initio* numerical outcome, and although a Fano-like lineshape of the electron transmission spectrum was observed in Ref. [4] both in the analytical model and in graphene, no explanation for this shape has been suggested and its relation to the properties of the N-states has not been considered. Here, we fill this gap by considering a simple model that elucidates a close connection of the N-resonance with that in the Fano model. We analytically show that the transmission amplitude near the resonances has a Fano character [28]

$$t(E) = t_0 \frac{E - E_0}{E - E_p + i\Gamma/2}, \quad (1)$$

where  $E_p - i\Gamma/2$  is the pole location in the complex energy plane, and  $E_0$  is the point of total reflection, the maximum transmissivity being unity. Real graphene will be shown to closely follow this formula.

Apart from the transmission probability  $T(E)$ , an important observable is the transmission timing. With the recent development of ultrashort laser pulses, the dynamics of Fano resonances in atoms was studied in real time [29–32]. It is characterized by the wave-packet group delay introduced by Bohm, Wigner, Eisenbud, and Smith [33–35] (Wigner time delay), which can be obtained as the energy derivative of the scattering phase  $\eta = \arg(t)$ ,

$$\Delta\tau = d\eta/dE \equiv \dot{\eta}. \quad (2)$$

Hartree atomic units  $\hbar = e = m_e = 1$  are used throughout the paper, so  $\Delta\tau$  is measured in the units of  $\hbar/1\text{Ha} = \hbar^3/m_e e^4 = 24.19$  as. Similar to the atomic case [30], the

resonant part of the delay is a Lorentzian function with the maximum at  $E_p$  and width  $\Gamma$ .

The paper is organized as follows. In Sec. II we introduce a 2D model for electron scattering on a 1D crystal (a thin wire) characterized by a sharp attractive potential in the  $\hat{y}$  direction and a weak corrugation along  $\hat{x}$ . We present the solution of the model in a general form, which is analyzed in the following sections. Section III discusses the system without corrugation in terms of eigenstates extended and localized in the  $\hat{y}$  direction. In Sec. IV, the corrugation is shown to couple the extended states with the localized ones of the same parity, which leads to Fano scattering resonances. The timing of the wave packet scattering is considered in Sec. V. In Sec. VI, the formalism is generalized to two identical wires. Sec. VII summarizes the results. The details of the calculations are given in Appendices A–E.

## II. INFINITELY THIN WIRE

To understand the physics of the resonance states [4], let us consider an infinite wire along the  $\hat{x}$  axis described

by a simple 2D Hamiltonian

$$\hat{H} = \frac{\hat{p}_x^2 + \hat{p}_y^2}{2} + \hat{V}, \quad (3)$$

$$\hat{V} = [2\Omega \cos(Kx) - \kappa]\delta(y) \quad (4)$$

An attractive potential  $\kappa > 0$  is modeled by a  $\delta$ -function in the  $\hat{y}$  direction and a weak corrugation  $\cos(Kx)$  along  $\hat{x}$ , where  $K = 2\pi/a$ , and  $a$  is the lattice constant. In the following we assume that  $|\Omega| \ll \kappa$  and consider the case  $\kappa < K$ , which somewhat simplifies the formulas. We will show that the continuous spectrum of the Hamiltonian (3) possesses sharp resonances at positive energies, which makes it similar to the Fano Hamiltonian  $\hat{H}_F$  of Ref. [28], see Eq. (A1) in Appendix A.

We consider the scattering of a normally incident wave, along  $\hat{y}$ . Similar to our previous work [36], we substitute the Laue representation for the scattering state

$$\Psi(\mathbf{r}) = \sum_g \phi_g(y) \exp(igx), \quad (5)$$

$$g = Kn, \quad n = 0, \pm 1, \pm 2, \dots$$

into both sides of the Lippmann-Schwinger equation

$$\Psi(\mathbf{r}) = \exp(ik_y y) + \delta\Psi(\mathbf{r}) \quad (6)$$

$$\delta\Psi(\mathbf{r}) = \iint d\mathbf{r}' G_0(\mathbf{r} - \mathbf{r}'; E) \hat{V}(\mathbf{r}') \Psi(\mathbf{r}') = \int dx' G_0(x - x', y; E) [2\Omega \cos(Kx') - \kappa] \Psi(x', 0), \quad (7)$$

where  $E = k_y^2/2$  and  $G_0$  is the free-electron Green's function,

$$G_0(\mathbf{r}; E) = \iint \frac{d\mathbf{q}}{4\pi^2} \frac{\exp(i\mathbf{q}\mathbf{r})}{E - q^2/2}. \quad (8)$$

After the integration over  $x'$  and  $\mathbf{q}$  Eq. (6) reduces to an algebraic equation

$$\Psi(\mathbf{r}) = \sum_g \phi_g(y) \exp(igx) = \exp(ik_y y) + \sum_g \exp(igx) G_{1D}(y, E - g^2/2) [\Omega(\phi_{g-K} + \phi_{g+K}) - \kappa\phi_g], \quad (9)$$

where  $\phi_g \equiv \phi_g(y=0)$  and  $G_{1D}(y, E)$  is the free-electron Green's function in 1D [37]

$$G_{1D}(y, E) = \begin{cases} -\frac{\exp(-k_0|y|)}{k_0}, & E < 0, \\ -\frac{i \exp(ik_0|y|)}{k_0}, & E > 0, \end{cases} \quad (10)$$

$$k_0 \equiv \sqrt{2|E|}. \quad (11)$$

It follows from Eq. (10) that the  $y \rightarrow \pm\infty$  asymptotics of the scattering function  $\Psi(\mathbf{r})$  of Eq. (9) contains only propagating waves with the positive energetic argument  $E - g^2/2$ . Thus, in the asymptotic region, the sum over  $g$  contains only finite number of terms with  $g^2 < 2E = k_y^2$ .

In particular, for  $k_y < K$ , i.e., for  $E < E_{\text{SB}} = K^2/2$  it contains only the central beam,  $g = 0$ ,

$$\phi_0(y) = \exp(ik_y y) + G_{1D}(y, E) [\Omega(\phi_{-K} + \phi_K) - \kappa\phi_0]. \quad (12)$$

Above  $E_{\text{SB}}$ , secondary beams emerge, with  $g > 0$ . In other words, the  $g > 0$  terms in Eq. (9) become propagating waves. We equate the coefficients of the Fourier harmonics  $\exp(igx)$  in Eq. (9) for  $y = 0$  and obtain the recurrence relation for the coefficients  $\phi_g$ :

$$\phi_g(1 + \kappa F_g) = \delta_{g,0} + \Omega F_g (\phi_{g-K} + \phi_{g+K}), \quad (13)$$

$$F_g \equiv \zeta_g^{-1} \equiv G_{1D}(0, E - g^2/2). \quad (14)$$

The solution of the infinite three-term recurrence relation (13) has the form of a continued fraction [38, 39]:

$$\phi_K = \frac{\Omega\phi_0}{\zeta_K + \kappa - \Omega^2\theta_2}, \quad (15)$$

$$\phi_0 = \frac{\zeta_0}{\zeta_0 + \kappa - \frac{2\Omega^2}{\zeta_K + \kappa - \Omega^2\theta_2}}, \quad (16)$$

where  $\theta_2$  is the second-step terminator of the continued fraction (16),

$$\theta_2 = \frac{1}{\zeta_{2K} + \kappa - \frac{\Omega^2}{\zeta_{3K} + \kappa - \frac{\Omega^2}{\ddots}}}, \quad (17)$$

see the derivation in Appendix B. Due to the symmetry of the Hamiltonian, the scattering solution is an even function of  $x$ ,  $\Psi(-x, y) = \Psi(x, y)$ , so the coefficients of the Laue representation (9) satisfy the relation  $\phi_{nK} = \phi_{-nK}$ . They can be calculated with any desired accuracy. By truncating the chain, i.e., by putting  $\phi_{n_0K} = 0$  at some  $n_0$ , we obtain approximate values of  $\phi_{nK}$  for  $n < n_0$ .

To obtain the functions  $F_g$  we substitute Eq. (10) into Eq. (14). For propagating  $g$ -beams  $F_g$  are purely imaginary, in particular, for the central beam it is

$$F_0 = -i/k, \quad (18)$$

and for  $E < E_{\text{SB}}$  all the other  $F_g$  are real,

$$F_{nK} = -1/\sqrt{(nK)^2 - k^2}, \quad n > 0. \quad (19)$$

The wave function for the central beam is

$$\begin{aligned} \phi_0(y) &= \exp(ik_y y) + r \exp(ik_y |y|) \\ &= \begin{cases} \exp(ik_y y) + r \exp(-ik_y y), & y \rightarrow -\infty, \\ t \exp(ik_y y), & y \rightarrow +\infty, \end{cases} \end{aligned} \quad (20)$$

where  $r \equiv |r| \exp(i\eta_R)$ ,  $t \equiv |t| \exp(i\eta_T)$  are the reflection and transition complex amplitudes. From Eq. (12) we obtain

$$r = F_0 (2\Omega\phi_K - \kappa\phi_0), \quad t = 1 + r. \quad (22)$$

The energy dependence of the scattering phase shifts  $\eta_R$  and  $\eta_T$  determines the Wigner time delays of the reflected  $\Delta\tau_R$  and transmitted  $\Delta\tau_T$  wave packets, see Eq. (2).

### III. BOUND STATES ABOVE VACUUM LEVEL

Besides the propagating states, which are expressed by Eq. (9), the Schrödinger equation has solutions bound in the  $\hat{y}$  direction. These states can be found from the

Lippmann-Schwinger equation (6) without the incident wave  $\Psi(\mathbf{r}) = \delta\Psi(\mathbf{r})$  with  $\delta\Psi(\mathbf{r})$  given by Eq. (7).

Let us first neglect the corrugation, i.e., set  $\Omega = 0$  in Eq. (4). In this case the recurrence relation (13) reduces to  $\phi_g(1 + \kappa F_g) = 0$  and has nontrivial solutions  $\phi_B \neq 0$  for energies  $E_B(g) = (g^2 - \kappa^2)/2$  at which  $1 + \kappa F_g = 0$ , so

$$\phi_B(y) = -\kappa G_{1D} \left( y, E_B(g) - \frac{g^2}{2} \right) \phi_B = \sqrt{\kappa} e^{-\kappa|y|}, \quad (23)$$

where  $\sqrt{\kappa}$  is a normalization coefficient. The wave function  $\phi_B(y)$  does not depend on  $g$  because  $E_B(g) - g^2/2 = -\kappa^2/2$ . For  $g^2 > \kappa^2$  these states have positive energies and are bound in  $\hat{y}$  direction. Indeed, for  $\Omega = 0$  the motions along  $\hat{x}$  and  $\hat{y}$  are independent. The wave functions are a product of the plane waves  $\exp(ik_x x)$  propagating along  $\hat{x}$  and the eigenstates of the 1D Hamiltonian of the motion along  $\hat{y}$

$$\hat{H}_y = \frac{\hat{p}_y^2}{2} - \kappa\delta(y). \quad (24)$$

The eigenstates include one bound state  $\phi_B(y)$  at the energy  $E_B = -\kappa^2/2$ . This yields the eigenstates of the full 2D Hamiltonian  $\hat{H} = \hat{p}_x^2/2 + \hat{H}_y$  that are bound in the  $\hat{y}$  direction and propagate along  $\hat{x}$ ,

$$\psi_B(k_x, \mathbf{r}) = \exp(ik_x x) \phi_B(y). \quad (25)$$

For a particular case of  $k_x = 0$  the bound states with energies  $E_B(g) = (g^2 - \kappa^2)/2$  have been obtained above from the Lippmann-Schwinger equation. For a general  $k_x$  their energy is  $E_B(k_x) = (k_x^2 - \kappa^2)/2$ .

Apart from the bound state  $\phi_B$ , see Eq. (23), the 1D Hamiltonian  $\hat{H}_y$  has the continuum eigenstates with positive energies  $E(k_y) = k_y^2/2$ , which may be odd  $\varphi^-(y) = \sqrt{2} \sin(k_y y)$  or even  $\varphi^+(y) = \sqrt{2} \cos(k_y |y| + \eta_{1D})$  under the reflection  $y \rightarrow -y$ . The phase shift  $\eta_{1D}$  is given by the equations

$$\cos(\eta_{1D}) = \frac{k_y}{\sqrt{k_y^2 + \kappa^2}}, \quad \sin(\eta_{1D}) = \frac{\kappa}{\sqrt{k_y^2 + \kappa^2}}. \quad (26)$$

The functions  $\varphi^-$  and  $\varphi^+$  multiplied by plane waves are then eigenstates of the full 2D Hamiltonian  $\hat{p}_x^2/2 + \hat{H}_y$  with positive energies  $E(\mathbf{k}) = k^2/2$ ,

$$\psi^p(\mathbf{k}, \mathbf{r}) = \exp(ik_x x) \varphi^p(k_y, y), \quad (27)$$

where  $p = \pm$  is the parity index.

In the left panel of Fig. 1, the band structure is depicted in the extended zone scheme. The right panel of Fig. 1 shows the same plot in the reduced zone scheme for an artificial periodicity in the  $\hat{x}$  direction. For a given crystal momentum  $k_x$  in the first Brillouin zone the spectrum contains discrete bound states  $\psi_B(k_n, \mathbf{r})$ ,  $k_n = k_x + Kn$  and continuum of even  $\psi^+(k_n, k_y, \mathbf{r})$  and odd  $\psi^-(k_n, k_y, \mathbf{r})$  extended states with continuously varying  $k_y$ .

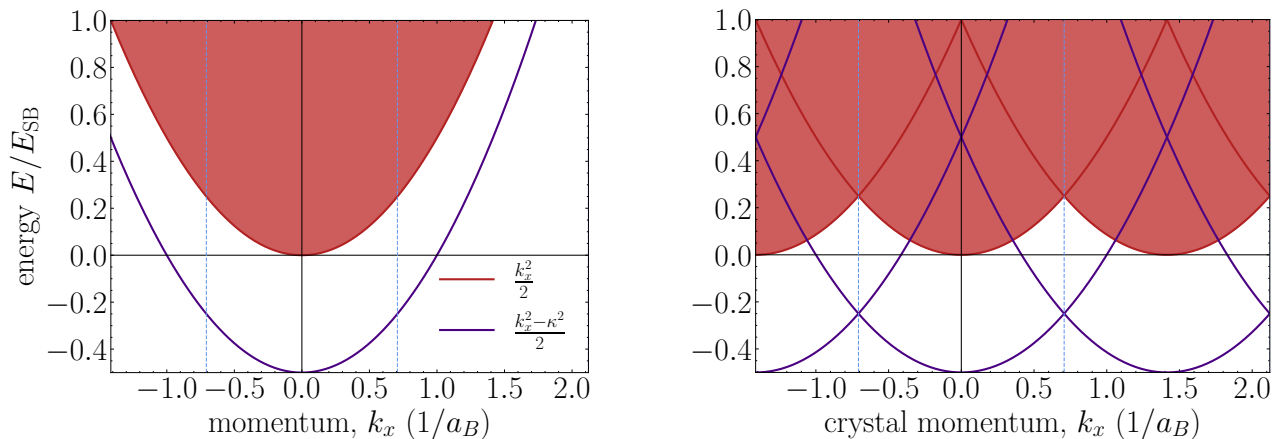


FIG. 1. Band structure of the model in the extended (left panel) and reduced (right panel) zone schemes in the absence of corrugation,  $\Omega = 0$ . Other parameters of the model are  $K = \sqrt{2}/a_B$ ,  $\kappa = 1/a_B$ .

The states  $\psi^+(\mathbf{k}, \mathbf{r})$  and  $\psi^-(\mathbf{k}, \mathbf{r})$  may be combined to form scattering states. In the absence of the corrugation, the normally incident wave produces only the specularly reflected beam, and the scattering states have the form (20). For  $\Omega = 0$ , the chain of equations (13) contains only the first equation with  $g = 0$ ,

$$\phi_0 \Big|_{\Omega=0} = \frac{1}{1 + \kappa F_0}.$$

Equation (22) gives the transmission coefficient

$$t_0 = \frac{1}{1 + \kappa F_0} = \frac{k_y}{k_y - i\kappa} = \cos(\eta_{1D})e^{i\eta_{1D}}, \quad (28)$$

which is a smooth function of  $k_y$  and  $E$ .

The right panel of Fig. 1 shows that in the repeated zone scheme, for  $E_B(k_n) = E(\mathbf{k})$ , i.e.,  $k_n^2 - \kappa^2 = k^2$  the states  $\psi_B(k_n, \mathbf{r})$  are degenerate with the states  $\psi^p(\mathbf{k}, \mathbf{r})$ . As we will see in the next section, the corrugation couples the extended and the even bound state and transforms it into a Fano resonance, whereas the odd state remains bound in the  $\hat{\mathbf{y}}$  direction. In this case the transmission probability  $T = |t|^2$  acquires a characteristic Fano shape near the resonance, in contrast to the smooth behavior of  $T_0 = |t_0|^2$ .

#### IV. COUPLING BY UMKLAPP PROCESSES

The corrugation  $\hat{\Omega} = 2\Omega \cos(Kx)\delta(y)$  couples the bound states  $\psi_B(k_x, \mathbf{r})$  of Eq. (25) with the even extended states  $\psi^+(\mathbf{k}', \mathbf{r})$ , similar to the Fano Hamiltonian (A1) where the perturbation  $\hat{V}_F$  couples a discrete level with the continuum [28]:

$$\begin{aligned} & \iint [\psi^+(\mathbf{k}', \mathbf{r})]^* \hat{\Omega} \psi_B(k_x, \mathbf{r}) d^2\mathbf{r} \\ & = \omega_{kk'} [\delta(k_x + K - k'_x) + \delta(k_x - K - k'_x)], \end{aligned} \quad (29)$$

where  $\omega_{kk'} = 2\pi\Omega\sqrt{2\kappa} \cos \eta_{1D}$ . However, our case is more involved because  $\hat{\Omega}$  also has nonzero matrix elements between the states of the same kind.

Let us now consider a normally incident wave along  $\hat{\mathbf{y}}$ , i.e.,  $k'_x = 0$  and  $E(\mathbf{k}') = k_y'^2/2$ . Then  $\hat{\Omega}$  couples the continuous states  $\psi^+(0, k'_y, \mathbf{r})$  and the bound states  $\psi_B(\pm K, \mathbf{r})$  having the energy  $E_B(\pm K) = (K^2 - \kappa^2)/2$ . The resonance occurs near  $E_r = k_r^2/2 = E_B(\pm K)$ , where  $k_r^2 = K^2 - \kappa^2$ . Below, we will consider the simplest case

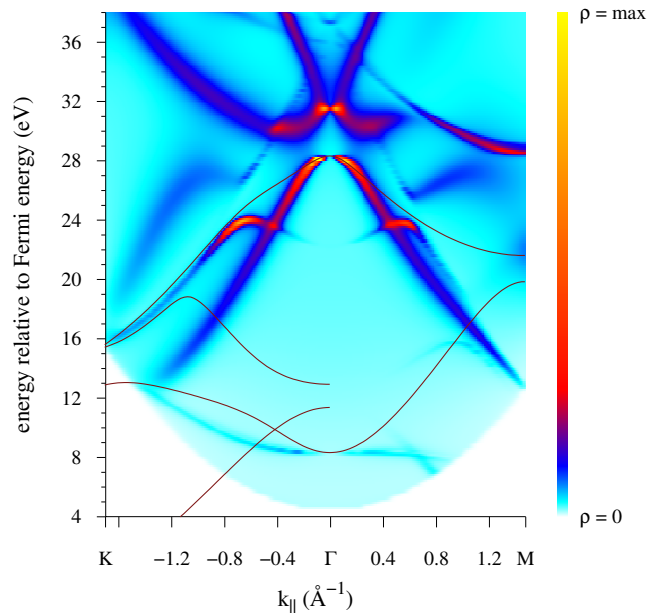


FIG. 2. Local spectral function  $\rho(E, \mathbf{k}_{\parallel})$  of the LEED states for graphene along the  $\Gamma M$  and  $\Gamma K$  lines.  $\rho(E, \mathbf{k}_{\parallel})$  characterizes the dwell time at the scatterer, which peaks at the resonances. The lines superimposed on the map show the dispersion of the strictly bound states, which are odd under reflection in the plane containing the  $\mathbf{k}_{\parallel}$  vector and the surface normal.

of  $\kappa < K$  and  $E_r < E_{\text{SB}}$ , i.e., the resonance in the energy range where only the central beam is present. The generalization to resonances at higher energies is straightforward.

In a real 3D crystal, the resonances manifest themselves as special features of the Bloch spectral function  $A(E, \mathbf{k}_{\parallel})$ , see Fig. 1 of Ref. [4]. However, for a strictly 2D crystal the  $A(E, \mathbf{k}_{\parallel})$  function depends on the artificial supercell lattice constant in the  $\hat{\mathbf{z}}$  direction. Thus, it is instructive to visualize the resonances in terms of the scattering states—the wave functions that describe the LEED experiment. For an electron of energy  $E$  and layer-parallel Bloch vector  $\mathbf{k}_{\parallel}$  incident from  $z = -\infty$  the color map in Fig. 2 shows the probability  $\rho(E, \mathbf{k}_{\parallel})$  to find the electron between the planes  $z = -1$  and  $4$  a.u. embracing the graphene layer located at  $z = 0$  (for the  $\rho(z, E)$  function at  $\mathbf{k}_{\parallel} = 0$  see Fig. 4(b) in Ref. [4]). The dispersion of the resonances is distinctly visible as the lines of enhanced dwell time at the scatterer.

Note that for the Hamiltonian (3) with a finite corrugation there exist states odd under the reflection  $x \rightarrow -x$ , which for  $E < E_{\text{SB}}$  are necessarily bound in the  $\hat{\mathbf{y}}$  direction. Indeed, for  $k'_x = 0$  the function  $\psi^+(0, k_y, \mathbf{r}) = \varphi^+(k_y, y)$  [see Eq. (27)] is obviously an even function of  $x$ . Thus, as follows from Eq. (29), the corrugation couples  $\psi^+$  only with the even combination  $\psi_{\text{B}}(K, \mathbf{r}) + \psi_{\text{B}}(-K, \mathbf{r}) = 2 \cos(Kx)\phi_{\text{B}}(y)$  of the bound states, whereas their odd combination  $\psi_{\text{B}}(K, \mathbf{r}) - \psi_{\text{B}}(-K, \mathbf{r}) = 2i \sin(Kx)\phi_{\text{B}}(y)$  remains unperturbed and confined in the  $\hat{\mathbf{y}}$  direction. The bound states with positive energy are a quite general phenomenon, beyond the present model. In particular, they exist in graphene, see Fig. 2.

Let us now calculate the transmission amplitude  $t$  using the approximate solution of the recurrence (13). Substituting  $\phi_K$  and  $\phi_0$  from Eqs. (15) and (16), respectively, into Eq. (22) we obtain after some algebra

$$t = t_0(k_y) \frac{\zeta_K + \kappa - \Omega^2 \theta_2}{\zeta_K + \kappa - \Omega^2 \theta_2 - 2\Omega^2 F_0 / (1 + \kappa F_0)},$$

and substituting  $F_0$  from Eq. (18) we finally obtain

$$t = t_0(k_y) \frac{\zeta_K + \kappa - \Omega^2 \theta_2}{\zeta_K + \kappa - \Omega^2 \theta_2 - \frac{2\Omega^2 \kappa}{k^2 + \kappa^2} + \frac{2i\Omega^2 k}{k^2 + \kappa^2}}. \quad (30)$$

In the absence of the corrugation,  $\Omega = 0$ , the amplitude  $t = t_0(k_y)$  is a smooth function of energy, see Eq. (28), and the corrugation drastically changes its behavior: The amplitude  $t$  acquires a Fano character near the resonance energy  $E_r = k_r^2/2$ , which we now demonstrate based on Eq. (30). Let us consider the energy range  $k < K$  where  $F_{nK}$  are real for all  $n > 0$ , see Eq. (19). For simplicity, we consider a sufficiently weak potential,  $\kappa < K$ . At the resonance, the sum  $\zeta_K + \kappa$  goes through zero, so in its vicinity,  $E - E_r \ll \kappa$ , the Taylor expansion holds:

$$\zeta_K + \kappa = \kappa - \sqrt{\kappa^2 - 2(E - E_r)} \approx (E - E_r)/\kappa, \quad (31)$$

which immediately yields

$$t \approx t_0(k_r) \frac{E - E_0}{E - E_p + i(\Gamma/2)}. \quad (32)$$

This approximate expression for the transmission amplitude has the canonical form (1) of the Fano resonance [28] with the parameters

$$E_0 = E_r + \kappa \Omega^2 \theta_2(E_r), \quad (33)$$

$$E_p = E_0 + \frac{2\Omega^2 \kappa^2}{k_r^2 + \kappa^2} = E_0 + \frac{2\Omega^2 \kappa^2}{K^2}, \quad (34)$$

$$\frac{\Gamma}{2} = \frac{2\kappa k_r \Omega^2}{k_r^2 + \kappa^2} = \frac{2\kappa k_r \Omega^2}{K^2}. \quad (35)$$

Note that  $\theta_2$  is a smooth function of energy, see Eq. (17), so it can be approximated by its value at  $E_r$ .

Near the resonance, the transmissivity is

$$T = |t|^2 = T_0(k_r) \frac{(E - E_0)^2}{(E - E_p)^2 + (\Gamma/2)^2}, \quad (36)$$

where  $T_0(k_y) = k_y^2 / (k_y^2 + \kappa^2)$  is the transmissivity in the absence of the corrugation, according to Eq. (28). This allows us to express the relation between the parameters in terms of the transmissivity:

$$E_p - E_0 = \frac{2\Omega^2 \kappa^2}{k_r^2} T_0(k_r), \quad (37)$$

$$\frac{\Gamma}{2} = \frac{2\kappa \Omega^2}{k_r} T_0(k_r). \quad (38)$$

The maximum of the Fano curve is related to the Fano lineshape asymmetry

$$q_{\text{F}} \equiv (E_p - E_0) / (\Gamma/2), \quad (39)$$

as  $T_{\text{max}} = T_0(q_{\text{F}}^2 + 1)$ , see Appendix C. From the expressions (37) and (38) for  $E_p - E_0$  and  $\Gamma$ , respectively, we obtain  $q_{\text{F}} = \kappa/k_r$ , so

$$T_{\text{max}} = T_0(k_r) \left[ \left( \frac{\kappa}{k_r} \right)^2 + 1 \right] = 1. \quad (40)$$

which proves that it is a point of complete transparency. The maximum is reached at  $E_{\text{max}} = E_p + \Gamma/2q_{\text{F}}$ , and the distance between the points of total reflectivity and complete transparency is  $E_{\text{max}} - E_0 = 2\Omega^2$ . Figure 3(a) shows the transmissivity for  $|E_{\text{B}}| = \kappa^2/2 = 6.54$  eV, which brings the energy  $E_0$  close to its location in graphene, see Fig. 4(a). To reproduce the width of the resonance in graphene we must set  $\Omega^2 = 1.88$  eV, Fig. 3(a). This value is too large to be considered a small perturbation,  $\Omega/\kappa = 0.38$ : the  $T(E)$  maximum  $E_{\text{max}} = 30.06$  eV occurs rather far from  $E_r = 26.91$  eV, and the approximation (31) becomes less accurate around  $E_{\text{max}}$ . As a result, the curve given by Eq. (36) visibly deviates from the exact  $T(E)$ . For a weaker corrugation,

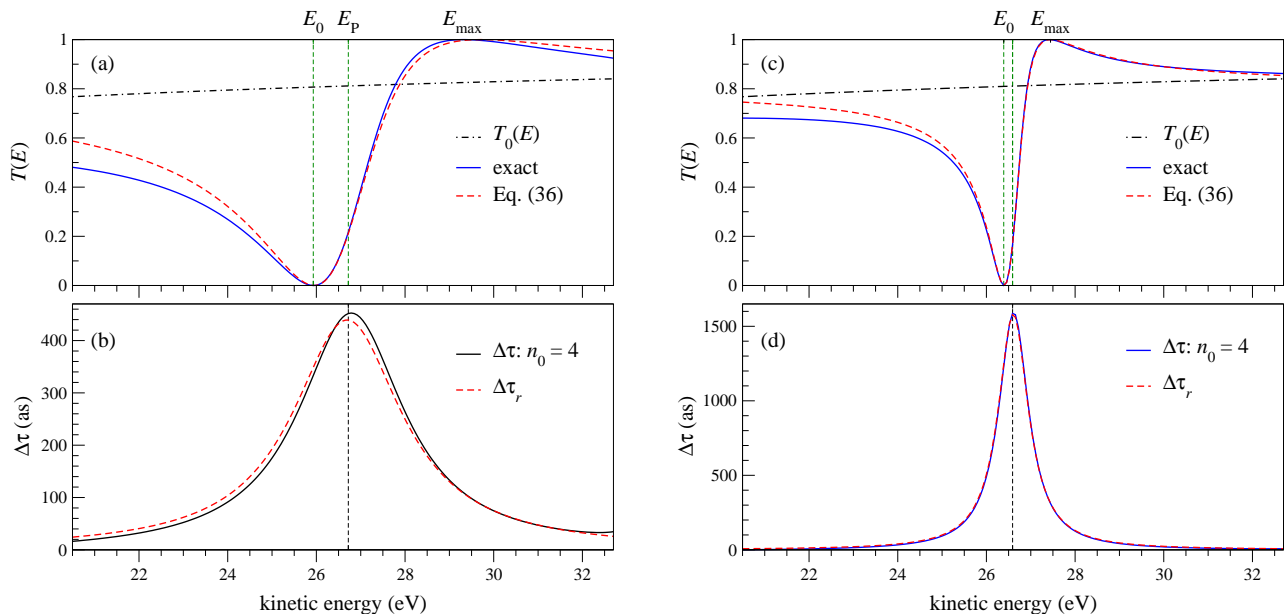


FIG. 3. (a) and (c) Energy dependence of the transmissivity for the Hamiltonian (3) with the corrugation parameters  $\Omega/\kappa = 0.38$  (a) and  $0.2$  (c), see Eq. (30). The structureless dash-dotted curve is the transmissivity in the absence of the corrugation,  $T_0(E) = 2E/(2E + \kappa^2)$ . Solid lines come from a numerically exact calculation of  $\theta_2$  in Eq. (17). The truncation of the chain (13) at  $n_0 = 3$  and  $4$  yields visually indistinguishable curves. Dashed curves are the approximation by Eq. (32). (b) and (d) Wigner time delay  $\Delta\tau_T$  (solid line) and its resonant part  $\Delta\tau_r$  (dashed line), see Eq. (43). Vertical dashed line shows the real part of the energy pole  $E_r$ , Eq. (34). The model parameters are the same as in graphs (a) and (c), respectively.

$\Omega = 0.2\kappa$ , the two curves coincide over an energy interval much wider than  $E_{\max} - E_0$ , see Fig. 3(c).

Figure 4(a) compares the *ab initio* transmissivity  $T$  for the graphene monolayer [4, 36] with the Fano function. The Fano parameters  $E_0 = 26.00$  eV,  $E_p = 27.90$  eV, and  $\Gamma = 3.76$  eV are calculated from the energies of the minimum of the *ab initio* curve  $E_0 = 26.00$  eV, its maximum  $E_{\max} = 29.73$  eV, and the midpoint  $E_{\text{mid}} = 27.89$  eV, where  $T$  reaches the half-maximum, as explained in Appendix C, in particular see Eq. (C6) for  $\Gamma$  and Eq. (C7) for  $E_p$ . As in the model, in the *ab initio* curve the maximum is the point of complete transparency.

## V. WIGNER TIME DELAY

The Wigner time delay  $\Delta\tau$  is defined as the difference in the time of arrival of a free particle and a scattered one in a region far from the scatterer. For a spectrally narrow wave packet the delay equals the energy derivative of the scattering phase [33–35], see Eq. (2). In our model, the transmission amplitude is the product of the amplitude  $t_0$  in the absence of the corrugation and the resonant part due to the corrugation-induced coupling, see Eqs. (28),

(29), and (30). Thus, the phase  $\eta_T = \arg(t)$  is the sum

$$\eta_T = \eta_{1D} + \eta_r,$$

$$\tan \eta_r = -\frac{2\Omega^2 k}{(k^2 + \kappa^2) [\zeta_K + \kappa - \Omega^2 \theta_2] - 2\Omega^2 \kappa} \quad (41)$$

$$\approx -\frac{\Gamma}{2(E - E_p)}. \quad (42)$$

The approximate equality (42) follows from Eq. (32) and is valid in the vicinity of the resonance. Hence, the delay is  $\Delta\tau_T = \Delta\tau_0 + \Delta\tau_r$ , and the resonant part  $\Delta\tau_r = \eta_r$  has a simple Lorentzian form near  $E_p$ :

$$\eta_r \approx \frac{\Gamma}{2[(E - E_p)^2 + (\Gamma/2)^2]}. \quad (43)$$

The exact general expression for  $\Delta\tau_r$  for  $E < K^2/2$  is presented in Appendix D.

The energy dependence of the time delay for our 2D model is shown in Figs. 3(b) and 3(d). This model turns out to rather accurately describe the time delay of the wave packet transmitted through graphene, as demonstrated in Fig. 4(b). Using the parameters of the Fano function extracted from the *ab initio*  $T(E)$  curve of Fig. 4(a) we obtain quantitative agreement between the *ab initio* and the model  $\Delta\tau(E)$  curves. The difference between them is the non-resonant contribution  $\Delta\tau_0$ . The maxima of both curves are at  $E_p \approx 27.9$  eV, which is the real part of the amplitude pole energy. Moreover, the maximum of the local spectral function  $\rho(E, \mathbf{k}_{\parallel} = 0)$

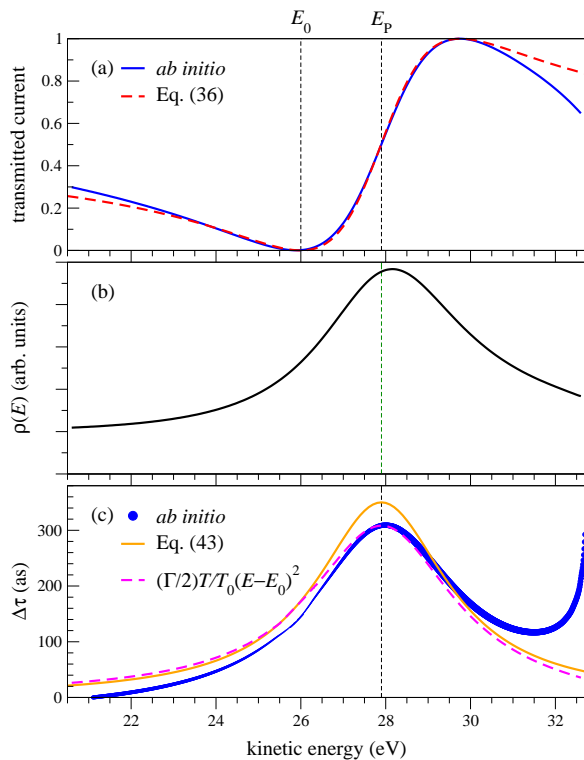


FIG. 4. (a) Transmissivity  $T(E)$  of graphene (solid line) and the Fano function of Eq. (36) (dashed line) for the model parameters  $E_0 = 26$  eV,  $\Gamma = 3.76$  eV, and  $E_p = 27.9$  eV, see Appendix C. (b) Wigner time delay  $\Delta\tau_T$  for scattering on graphene [solid line of variable thickness proportional to  $T(E)$ ] and delay  $\Delta\tau_T$  obtained from the Fano function with the same parameters as in graph (a) (thin line). Dashed line shows  $\Delta\tau$  derived from the *ab initio*  $T(E)$  curve according to Eqs. (36) and (43):  $\Delta\tau = (\Gamma/2)T(E)/T_0(E - E_0)^2$  assuming  $T_0 = 0.5$ . Vertical dashed line shows the real part of the energy pole  $E_p$ , see Eq. (34). (c) Spectral function  $\rho(E, \mathbf{k}_{\parallel})$  of the scattering states for  $\mathbf{k}_{\parallel} = 0$ , see Fig. 2 and its caption.

is very close to  $E_p$ , and its width is close to that of the  $\Delta\tau(E)$  peak, see Fig. 4(c).

## VI. TWO PARALLEL WIRES

For multiple wires, the interference between waves transmitted and reflected from individual scatterers drastically modifies the energy dependence of the transmission probability and the time delay [36]. In this case, Eq. (9) is replaced with a system of equations, generally

one equation per wire. Here, we consider two identical wires and make use of the symmetry of the Hamiltonian, whereby the two equations decouple. The Hamiltonian for two wires reads

$$\hat{H}_2 = \frac{\hat{p}_x^2 + \hat{p}_y^2}{2} + \hat{V}_2, \quad (44)$$

$$\hat{V}_2 = [2\Omega \cos(Kx) - \kappa] \left[ \delta\left(y - \frac{a}{2}\right) + \delta\left(y + \frac{a}{2}\right) \right], \quad (45)$$

and we again assume that  $|\Omega| \ll \kappa$ .

In the absence of the corrugation, two states bound within the structure appear, so two resonances could be expected. (Their energies and wave functions are calculated in Appendix E). Due to the symmetry of the Hamiltonian, its eigenfunctions may be chosen to be even or odd functions of both coordinates. For the plane wave incident along  $\hat{y}$  it is sufficient to consider only the eigenfunctions that are even under the reflection  $x \rightarrow -x$  and may be even or odd in the  $y$  variable,  $\Psi^p(x, -y) = p\Psi^p(x, y)$ . The subspaces of even and odd functions are orthogonal, and the Lippmann-Schwinger equation may be solved for functions in each subspace separately. The coefficients of Laue representations for the scattering states acquire additional index  $p$  for even  $p = +$  and odd  $p = -$  functions,

$$\Psi^p(\mathbf{r}) = \sum_g \phi_g^p(y) \exp(igx). \quad (46)$$

The Lippmann-Schwinger equation now has the form

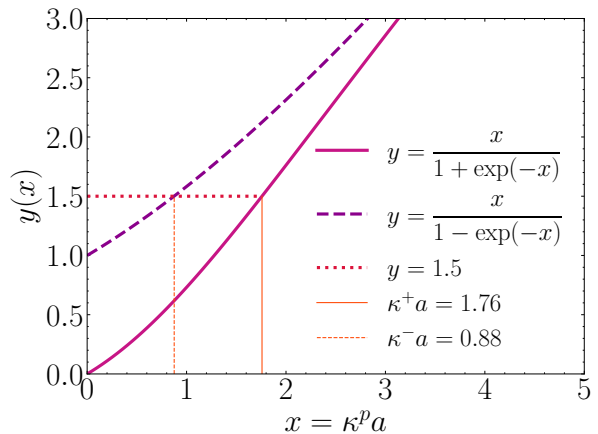


FIG. 5. The bound state energy parameter  $\kappa^p = \sqrt{2|E_B^p|}$  is determined from the intersection of the curve  $y(x) = x/[1 + p \exp(-x)]$  with the horizontal line  $y(x) = \kappa a$ . Odd bound states,  $p = -$ , exists only for  $\kappa a > 1$ .

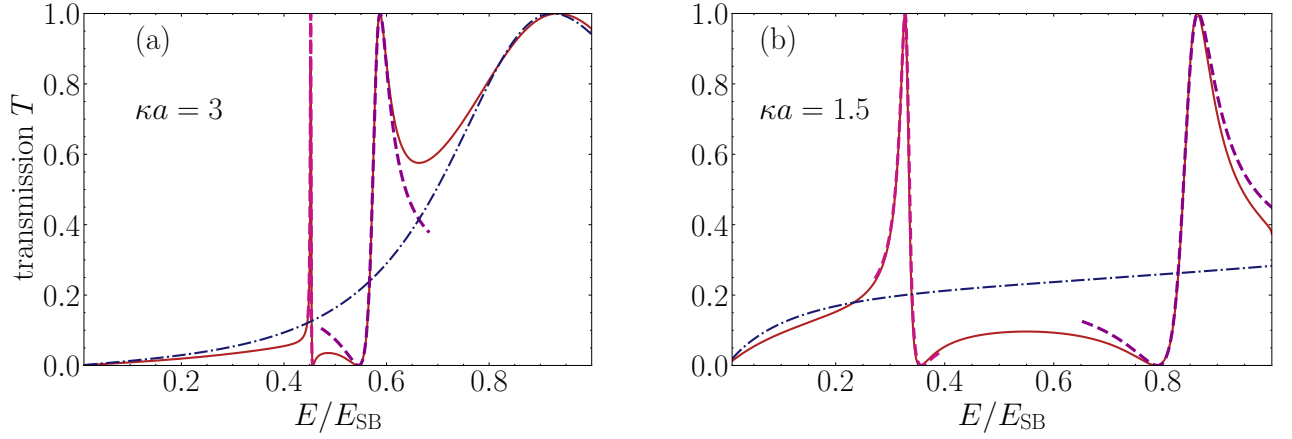


FIG. 6. Energy dependence of the transmissivity  $T = |t|^2$  by Eq. (56) for the model Hamiltonian  $\hat{H}_2$  of Eq. (44). Solid line shows a numerically exact calculation of  $\theta_2^p$ . The truncation of the chain (13) at  $n_0 = 3$  yields a visually indistinguishable curve. The blue dash-dotted curve is the transmissivity for the absence of corrugation. The approximate  $T(E)$  in the vicinity of resonance by Eq. (60) are shown by the dashed curves.

$$\Psi^p(\mathbf{r}) = \Psi_0^p(y) + \delta\Psi^p(\mathbf{r}) \quad (47)$$

$$\begin{aligned} \delta\Psi^p(\mathbf{r}) &= \iint d\mathbf{r}' G_0(\mathbf{r} - \mathbf{r}'; E) \hat{V}_2(\mathbf{r}') \Psi^p(\mathbf{r}') \\ &= \int dx' [2\Omega \cos(Kx') - \kappa] \left[ G_0\left(x - x', y - \frac{a}{2}; E\right) + pG_0\left(x - x', y + \frac{a}{2}; E\right) \right] \Psi^p\left(x', \frac{a}{2}\right), \end{aligned} \quad (48)$$

where the factor  $p$  is 1 for even and  $-1$  for odd functions. The unperturbed function  $\Psi_0^p(y)$  in Eq. (47) may be an even  $\Psi_0^+(y) = \cos(k_y y)$  or an odd  $\Psi_0^-(y) = \sin(k_y y)$  eigenfunction for  $k_x = 0$  of the free motion Hamiltonian  $\hat{H}_0 = (\hat{p}_x^2 + \hat{p}_y^2)/2$ . The corresponding Green's function  $G_0$  is given by Eq. (8). The integration over  $x'$  in Eq. (48) and over  $\mathbf{q}$  in Eq. (8) reduce the integral equation (47) to the algebraic equation

$$\begin{aligned} \Psi^p(\mathbf{r}) &= \sum_g \phi_g^p(y) \exp(igx) = \Psi_0^p(y) + \\ &\sum_g \exp(igx) \left[ \Omega (\phi_{g-K}^p + \phi_{g+K}^p) - \kappa \phi_g^p \right] \left[ G_{1D}\left(y - \frac{a}{2}, E - \frac{g^2}{2}\right) + pG_{1D}\left(y + \frac{a}{2}, E - \frac{g^2}{2}\right) \right], \end{aligned} \quad (49)$$

where  $\phi_g^p \equiv \phi_g^p(a/2) = p\phi_g^p(-a/2)$ , and  $G_{1D}(y - y'; E)$  is the free-electron Green's function in 1D [37], see Eq. (10). Similar to the case of a single wire, the sum over  $g$  in the asymptotic regions  $y \rightarrow \pm\infty$  contains only finite number of terms with  $g^2/2 < E$ . In particular, for  $k_y < K$ , i.e., for the energies below  $E_{\text{SB}} = K^2/2$ , it contains only the central beam,  $g = 0$ :

$$\phi_0^p(y) = \Psi_0^p(y) + \left[ G_{1D}\left(y + \frac{a}{2}, E\right) + pG_{1D}\left(y - \frac{a}{2}, E\right) \right] \left[ \Omega (\phi_{-K}^p + \phi_K^p) - \kappa \phi_0^p \right]. \quad (50)$$

As in the single-wire case, equating the coefficients of the Fourier harmonics  $\exp(igx)$  in Eq. (49) for  $y = 0$  leads to the recurrence relation for  $\phi_g^p$

$$\phi_g^p(1 + \kappa F_g^p) = \delta_{g0} \Psi_0^p\left(\frac{a}{2}\right) + \Omega F_g^p (\phi_{g-K}^p + \phi_{g+K}^p), \quad (51)$$

$$F_g^p \equiv \frac{1}{\zeta_g^p} \equiv G_{1D}\left(0, E - \frac{g^2}{2}\right) + pG_{1D}\left(a, E - \frac{g^2}{2}\right).$$

The solution of the recurrence is similar to the relations

(13), see Appendix B, and it yields the perturbed solutions for the even and odd standing waves.

Let us now consider a normally incident wave, for which the scattering function is the combination

$$\begin{aligned} \Psi(\mathbf{r}) &= \Psi^+(\mathbf{r}) + i\Psi^-(\mathbf{r}) \\ &= \exp(iky) + \delta\Psi^+(\mathbf{r}) + i\delta\Psi^-(\mathbf{r}) \end{aligned} \quad (52)$$



The wave function for the central beam is

$$\Psi_c(\mathbf{r}) = \phi_0^+(y) + i\phi_0^-(y) \quad (53)$$

$$= \begin{cases} \exp(iky) + r_2 \exp(-iky) & y \rightarrow -\infty \\ t_2 \exp(iky) & y \rightarrow +\infty \end{cases}, \quad (54)$$

where  $r_2$  and  $t_2$  are the reflection and transmission amplitudes

$$r_2 = -\frac{2i}{k} \left\{ \cos \frac{ka}{2} \tilde{\phi}^+ - \sin \frac{ka}{2} \tilde{\phi}^- \right\}, \quad (55)$$

$$t_2 = 1 - \frac{2i}{k} \left\{ \cos \frac{ka}{2} \tilde{\phi}^+ + \sin \frac{ka}{2} \tilde{\phi}^- \right\}, \quad (56)$$

$$\tilde{\phi}^p \equiv 2\Omega\phi_K^p - \kappa\phi_0^p. \quad (57)$$

The coefficients  $\phi_K^p$  and  $\phi_0^p$  can be expressed as the continued fraction of the same form as Eqs. (15) and (16), respectively, with the functions  $\zeta_g$  and  $\theta_2$  replaced by  $\zeta_g^p$  and  $\theta_2^p$ . Substituting the resulting expressions for  $\phi_K^p$  and  $\phi_0^p$  into Eq. (57) we obtain after some algebra

$$\tilde{\phi}^p = \frac{\Psi_0^p\left(\frac{a}{2}\right) [2\Omega^2 - \kappa(\zeta_K^p + \kappa - \Omega^2\theta_2^p)]}{(\zeta_K^p + \kappa - \Omega^2\theta_2^p)(1 + \kappa F_0^p) - 2\Omega^2 F_0^p}, \quad (58)$$

$$F_0^p = -\frac{i}{k}[1 + p \exp(ika)].$$

In order to simplify the expression (58), we note that for  $\Omega = 0$  it takes the form

$$\tilde{\phi}_0^p = -\frac{\kappa\Psi_0^p\left(\frac{a}{2}\right)}{(1 + \kappa F_0^p)}, \quad (59)$$

so we can write  $\tilde{\phi}^p = \tilde{\phi}_0^p \tilde{\phi}_r^p$ , where

$$\tilde{\phi}_r^p \equiv \frac{\zeta_K^p + \kappa - \Omega^2(\theta_2^p + 2/\kappa)}{\zeta_K^p + \kappa - \Omega^2\theta_2^p - \frac{2\Omega^2 F_0^p}{1 + \kappa F_0^p}},$$

which in the vicinity of the resonance energy  $E_r^p \equiv (k_r^p)^2/2 = E_{\text{SB}} - E_B^p$  acquires the Fano shape

$$\tilde{\phi}_r^p \approx \frac{E - E_0^p}{E - E_p^p + i\Gamma^p/2}, \quad (60)$$

where  $E_B^p = -(\kappa^p)^2/2$  is the energy of the bound state of parity  $p$  at  $k_x = 0$  of the uncorrugated double-wire. The parameter  $\kappa^p$  satisfies the equation  $\kappa^p a/[1 + p \exp(-k^p a)] = \kappa a$ , see Appendix E. Its solution for  $\kappa a = 1.5$  is illustrated in Fig. 5. Let us now calculate the parameters  $E_0^p$ ,  $E_p^p$ , and  $\Gamma^p$  in Eq. (60). For  $(E - E_r^p)/\kappa \ll 1$  we have

$$\zeta_K^p + \kappa = \kappa - \frac{\sqrt{K^2 - k^2}}{1 + p \exp(-a\sqrt{K^2 - k^2})} \approx (E - E_r^p) \frac{\kappa C^p}{(\kappa^p)^2},$$

where we have introduced a dimensionless coefficient  $C^p \equiv 1 + p\kappa a \exp(-\kappa^p a)$ . This approximation gives for a given parity  $p = \pm$  the transmission minimum at

$$E_0^p = E_r^p + \frac{(\Omega\kappa^p)^2(\theta_2^p + 2/\kappa)}{\kappa C^p},$$

and the pole at the complex energy  $E_p^p + i\Gamma^p/2$  with  $E_p^p = E_0^p - u^p$  and  $\Gamma^p = 2v^p$ . Here  $u^p$  and  $v^p$  are the real and imaginary part of the quantity  $\frac{2(\Omega\kappa^p)^2}{\kappa^2 C^p(1 + \kappa F_0^p)}$ .

We see that the reflection and transmission amplitudes for the double-wire model, Eqs. (55) and (56), contain a linear combination of two Fano functions,  $\tilde{\phi}^+$  and  $\tilde{\phi}^-$ . Their interference gives a rather complicated transmissivity and reflectivity functions  $T_2(E)$  and  $R_2(E)$ , which depend in a complex way on the parameters of the potential  $\hat{V}_2$ , see Fig. 6. Apart from that, one can see in Fig. 6(a) an additional transmission resonance that is present both with and without corrugation, see the blue dash-dotted curve. These are the  $T = 1$  resonances due to the 1D motion that are the precursors of the energy bands of the crystal composed of the infinite number of the wires. They are caused by the interference of the multiple reflections between the wires.

## VII. CONCLUSION

We have demonstrated that the N-resonances in electron scattering on atomically thin layers occur due to the same mechanism as classical the Fano resonance, namely the coupling between the bound and extended states. It is thus not surprising that the transmissivity curve has the Fano shape. We have presented the mathematical proof and derived analytical expressions for the Fano parameters for the specific case of corrugated wires, which establish a functional relation between the complex energy of the resonance and the observed transmissivity. The *ab initio* calculations for graphene [4] have turned out to be fully consistent with this theory: We explained and quantitatively reproduced the results of Ref. [4], in other words, we have traced the observed scattering resonance to the existence of a strictly bound stationary state in an uncorrugated reference layer.

Furthermore, we have shown that the scattering phase exhibits dramatic variation with energy near the resonance, which results in a large Wigner time delay  $\Delta\tau$ . The *ab initio* calculation of  $\Delta\tau(E)$  for graphene has been found to closely follow the analytical theory and agree with the resonance shape inferred from the scattering spectral function.

The theory has been generalized to several wires (layers in the 3D case) arranged in a superstructure, whereby the bound states of the individual wires interact and the N-resonance splits. In this case the scattering amplitude has the Fano shape near each resonance, and the line-shape parameters depend in a rather complex way on the distance between the individual scatterers.

## ACKNOWLEDGMENTS

Fruitful discussions with V.U. Nazarov are gratefully acknowledged. This work was supported by

the Spanish Ministry of Science and Innovation (Projects No. PID2022-139230NB-I00 and No. PID2022-138750NB-C22) and by the National Academy of Sciences of Ukraine (Projects No. III-2-22 and No. III-4-23). D.E. and R.K. acknowledge support from Volkswagen Foundation through the project "Synthesis, theoretical investigation and experimental study of emergent iron-based superconductors".

### Appendix A: Fano Hamiltonian

It is instructive to apply the Green's function approach to the Fano Hamiltonian [28]

$$\hat{H}_F = \hat{H}_0 + \hat{V}_F, \quad (\text{A1})$$

$$\hat{H}_0 = |\varphi\rangle E_\varphi \langle\varphi| + \int_{E_\varphi-D}^{E_\varphi+D} |\psi_E\rangle E \langle\psi_E| dE, \quad (\text{A2})$$

$$\hat{V}_F = \int_{E_\varphi-D}^{E_\varphi+D} (|\varphi\rangle V_E^* \langle\psi_E| + |\psi_E\rangle V_E \langle\varphi|) dE, \quad (\text{A3})$$

where  $\hat{H}_0$  is the unperturbed Hamiltonian,  $|\varphi\rangle$  is the eigenfunction of its discrete energy level  $E_\varphi$  that lies within the energy range  $E_\varphi - D < E < E_\varphi + D$ , and  $|\psi_E\rangle$  are the eigenfunctions of the continuous spectrum normalized as  $\langle\psi_{E'}|\psi_E\rangle = \delta(E' - E)$ . The perturbation  $\hat{V}$  couples these states. The eigenstates  $|\Phi\rangle$  of  $\hat{H}_F$  of energy  $E$  satisfy the Lippmann-Schwinger equation

$$|\Phi\rangle = |\psi_E\rangle + \hat{G}_0(E + i0)\hat{V}|\Phi\rangle, \quad (\text{A4})$$

where

$$\hat{G}_0(\omega) = (\omega - \hat{H}_0)^{-1} = \frac{|\varphi\rangle \langle\varphi|}{\omega - E_\varphi} + \int_{E_\varphi-D}^{E_\varphi+D} \frac{|\psi_E\rangle \langle\psi_E|}{\omega - E} dE$$

$$|\Phi\rangle = |\psi_E\rangle + \frac{V_E^*}{E + i0 - E_\varphi - F(E)} \left[ |\varphi\rangle + \int_{E_\varphi-D}^{E_\varphi+D} \frac{V_{E'}}{E + i0 - E'} |\psi_{E'}\rangle dE' \right]. \quad (\text{A10})$$

It is easy to verify that  $\hat{H}_F |\Phi\rangle = E |\Phi\rangle$ .

is the resolvent of the unperturbed Hamiltonian, and we use the standard notation

$$f(E + i0) = \lim_{s \rightarrow 0^+} f(E + is).$$

Substituting

$$\hat{G}_0(\omega)\hat{V} = \int_{E_\varphi-D}^{E_\varphi+D} \left( \frac{|\varphi\rangle V_E^* \langle\psi_E|}{\omega - E_\varphi} + \frac{|\psi_E\rangle V_E \langle\varphi|}{\omega - E} \right) dE$$

into Eq.(A4) yields

$$|\Phi\rangle = |\psi_E\rangle + \int_{E_\varphi-D}^{E_\varphi+D} \left( \frac{|\varphi\rangle V_{E'}^* \langle\psi_{E'}|\Phi\rangle}{E + i0 - E_\varphi} + \frac{|\psi_{E'}\rangle V_{E'} \langle\varphi|\Phi\rangle}{E + i0 - E'} \right) dE'. \quad (\text{A5})$$

By multiplying Eq. (A5) from the left by  $\langle\varphi|$  we obtain

$$\langle\varphi|\Phi\rangle = \int_{E_\varphi-D}^{E_\varphi+D} \frac{V_{E'}^* \langle\psi_{E'}|\Phi\rangle}{E + i0 - E_\varphi} dE', \quad (\text{A6})$$

and the multiplication by  $\langle\psi_{E''}|$  gives

$$\langle\psi_{E''}|\Phi\rangle = \delta(E - E'') + \frac{V_{E''} \langle\varphi|\Phi\rangle}{E + i0 - E''}. \quad (\text{A7})$$

Upon substituting Eq. (A7) into Eq. (A6) we obtain

$$\langle\varphi|\Phi\rangle = \frac{V_E^*}{E + i0 - E_\varphi - F(E)}, \quad (\text{A8})$$

$$F(E) \equiv \int_{E_\varphi-D}^{E_\varphi+D} \frac{|V_{E'}|^2}{E + i0 - E'} dE'.$$

This gives

$$\langle\psi_{E''}|\Phi\rangle = \delta(E - E'') + \frac{V_{E''}}{E + i0 - E''} \frac{V_E^*}{E + i0 - E_\varphi - F(E)}. \quad (\text{A9})$$

Finally, we substitute Eqs. (A8) and (A9) into Eq. (A5) and obtain

---

Let us consider the  $r \rightarrow \infty$  asymptotic of  $\langle r|\Phi\rangle$ . The

eigenfunction of the discrete energy level is localized, and  $\langle r|\varphi\rangle \rightarrow 0$ . For the eigenstates that belong to the continuous spectrum, one have  $\langle r|\psi_{E'}\rangle \propto \sin[k(E')r + \delta]$ , where  $k(E') = \sqrt{2E'}$ ,  $\delta$  is a phase shift [28, 40]. It is reasonable to assume that the matrix element between the localized and extended functions  $V_{E'}$  decreases rapidly as a function of  $|E' - E_\varphi|$ . Then, passing to the integration over  $k$ , we may extend the limits of integration to  $\pm\infty$  and apply the residue theorem for the calculation of the integral [28]

$$\int_{-\infty}^{+\infty} \frac{V(k^2/2) \sin[k(E')r + \delta]}{E \pm i0 - k^2/2} k dk = -\pi V_E \cos[k(E)r + \delta].$$

Then

$$\begin{aligned} \langle r|\Phi\rangle &\propto \sin[k(E)r + \delta] - \frac{\pi|V_E|^2 \cos[k(E)r + \delta]}{E + i0 - E_\varphi - F(E)} \\ &\propto \sin[k(E)r + \delta + \Delta_r], \end{aligned}$$

where the resonance part of the phase shift is (cf. Eq. (15) of Ref. [28])

$$\Delta_r = -\arctan \frac{\pi|V_E|^2}{E - E_\varphi - F(E)} - \arctan \frac{\Gamma}{2(E - E_p)},$$

where  $\Gamma \equiv 2\pi|V_E|^2$  and  $E_p \equiv E_\varphi + F(E)$ . The sharp variation of the phase shift as  $E$  passes through the resonance energy  $E_p$  leads to a large Wigner time delay in a wave packet scattering, see Eq. (43).

## Appendix B: Calculation of coefficients $\phi_{nK}$

Let us find the solution of the recurrences (13) and (51). As mentioned in the main text, it follows from the symmetry of the scattering function that the coefficients of Laue expansions, Eqs. (5) and (46) obey the relation  $\phi_g = \phi_{-g}$ . Here we drop the superscript  $p$  in the recurrence terms of Eq. (51); it is easily restored in the final formulas. We rewrite the equations (13) and (51) as

$$\zeta_g + \kappa - \Omega \frac{\phi_{g+K}}{\phi_g} = \frac{\zeta_0 b_0}{\phi_0} \delta_{g0} + \frac{\Omega \phi_{g-K}}{\phi_g}, \quad (\text{B1})$$

where  $b_0 = 1$  in Eq. (13) and  $b_0 = \Psi_0^p(\frac{a}{2})$  in Eq. (51). For  $g = 0$ , Eq. (B1) gives

$$\phi_0 = \frac{b_0 \zeta_0}{\zeta_0 + \kappa - 2\Omega \frac{\phi_K}{\phi_0}}, \quad (\text{B2})$$

and for  $g > 0$  the recurrence is

$$\frac{\phi_g}{\phi_{g-K}} = \frac{\Omega}{\zeta_g + \kappa - \Omega \frac{\phi_{g+K}}{\phi_g}}. \quad (\text{B3})$$

Substituting these expressions for consequent  $g$  into Eq. (B2), we obtain the solution for  $\phi_0$  in the form of continued fraction

$$\phi_0 = \frac{b_0 \zeta_0}{\zeta_0 + \kappa - \frac{2\Omega^2}{\zeta_K + \kappa - \Omega \frac{\phi_{2K}}{\phi_K}}} = \frac{b_0 \zeta_0}{\zeta_0 + \kappa - 2\Omega^2 \theta_1}, \quad (\text{B4})$$

where the function  $\theta_1(E)$  is

$$\theta_1 = \frac{1}{\zeta_K + \kappa - \Omega^2 \theta_2}, \quad (\text{B5})$$

and for  $n > 1$  the recurrence reads

$$\theta_n = \frac{1}{\zeta_{nK} + \kappa - \Omega^2 \theta_{n+1}}. \quad (\text{B6})$$

Thus,  $\theta_1(E)$  is the continued fraction

$$\theta_1 = \frac{1}{\zeta_K + \kappa - \frac{\Omega^2}{\zeta_{2K} + \kappa - \frac{\Omega^2}{\zeta_{3K} + \kappa - \ddots}}}. \quad (\text{B7})$$

which can be calculated with any desired accuracy. We may truncate the chain by setting  $\phi_{n_0 K} = 0$ , i.e.,  $\theta_{n_0} = 0$ , at different  $n_0$ , for example:

$n_0 = 3$ : setting  $\phi_{3K} = 0$  and  $\theta_3 = 0$  yields

$$\theta_{1,3} \approx \frac{1}{\zeta_K + \kappa - \frac{\Omega^2}{\zeta_{2K} + \kappa}}; \quad (\text{B8})$$

$n_0 = 4$ : setting  $\phi_{4K} = 0$  and  $\theta_4 = 0$  yields

$$\theta_{1,4} \approx \frac{1}{\zeta_K + \kappa - \frac{\Omega^2}{\zeta_{2K} + \kappa - \frac{\Omega^2}{\zeta_{3K} + \kappa}}}. \quad (\text{B9})$$

Alternatively,  $\theta_1$  can be calculated by the modified Lentz's algorithm [41–43]. Then the function  $f \equiv 1/\theta_1$  is calculated by iterations

$$\begin{aligned} f_j &= f_{j-1} \Delta_j, \quad \Delta_j = C_j D_j, \\ C_j &= b_j + \frac{a_j}{C_{j-1}}, \quad D_j = \frac{1}{b_j + a_j D_{j-1}}, \quad j = 1, 2, \dots, \end{aligned}$$

where  $f_0 = C_0 = b_0$ ,  $D_0 = 0$ ,  $b_j = \zeta_{(j+1)K} + \kappa$ , and  $a_j = -\Omega^2$ . The iterations stop when  $|\Delta_j - 1| \approx 0$ . More details can be found in Refs. 41–43. It is the result of the iterative procedure that we have referred to as numerically exact.

Having calculated  $\theta_1$ , we obtain  $\phi_0$  from Eq. (B4). Comparing Eqs. (B4) and (B2), we see that  $\phi_K = \Omega \phi_0 \theta_1$ . The numerically exact transmissivity is depicted in Fig. 3 by solid line. The deviation of the approximations by Eq. (B8) or (B9) from the exact result is within the linewidth.

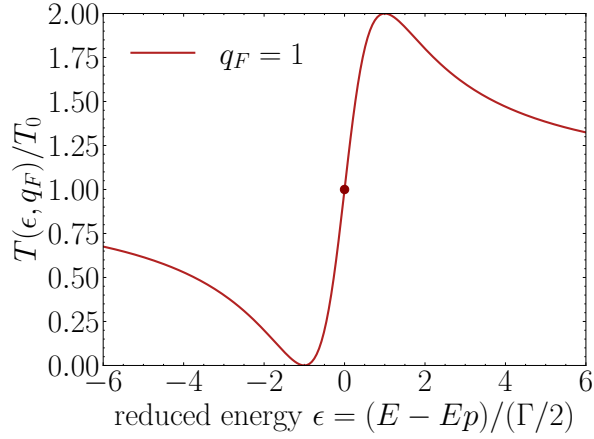


FIG. 7. Reduced transmission probability near the Fano resonance. The circle indicates the reduced energy  $\epsilon_{\text{mid}}$  at which  $T(\epsilon_{\text{mid}}) = T(\epsilon_{\text{max}})/2$ .

### Appendix C: Analysis of Fano resonance curve

Here we show how to infer the real and imaginary parts of the pole,  $E_p$  and  $\Gamma/2$ , from the energies of the minimum (zero) of the experimental curve  $E_0$ , its maximum  $E_{\text{max}}$ , and the point  $E_{\text{mid}}$ , where the transmissivity is half of its maximum. Near a Fano resonance, the transmission amplitude has the form given by Eq. (1). The transmissivity reads

$$T(E) = |t|^2 = T_0 \frac{(E - E_0)^2}{(E - E_p)^2 + (\Gamma/2)^2}. \quad (\text{C1})$$

From Eq. (1) we see that the amplitude has a pole at  $z = E_p - i\Gamma/2$ . Strictly speaking, the pole occurs in the analytic continuation of the amplitude to the lower complex-energy half-plane of the unphysical sheet of the Riemann surface (through the branch cut on the real axis for  $E \leq 0$ ).

If one obtains the curve  $T(E)$  from a (numerical) experiment, the parameters  $E_p$  and  $\Gamma$  are not known. Below, we show how they may be obtained from three characteristic features of the curve. Namely, the minimum (zero) of the experimental curve  $E_0$ , its maximum,  $E_{\text{max}}$  and the point  $E_{\text{mid}}$ , where  $T(E_{\text{mid}}) = T(E_{\text{max}})/2$ .

The expression (C1) is usually written as a function of the reduced variables  $q_F$  (39) and  $\epsilon$ :

$$T(\epsilon, q_F) = T_0 \frac{(\epsilon + q_F)^2}{\epsilon^2 + 1}, \quad (\text{C2})$$

$$\epsilon \equiv (E - E_p)/(\Gamma/2), \quad (\text{C3})$$

Figure 7 shows the reduced transmission probability  $T/T_0$  for  $q_F = 1$ . The curve is described by the three characteristic points: the minimum  $T(\epsilon_0, q_F) = 0$  at  $\epsilon_0 = -q_F$ , the maximum  $T(\epsilon_{\text{max}}, q_F) = T_0(q_F^2 + 1)$  at  $\epsilon_{\text{max}} = 1/q_F$ , and the midpoint  $T(\epsilon_{\text{mid}}, q_F) = T(\epsilon_{\text{max}}, q_F)/2$  at  $\epsilon_{\text{mid}} = (1 - q_F)/(1 + q_F)$ . Using the definitions (C3) and

(39), we obtain

$$\Delta_m = E_{\text{max}} - E_0 = \frac{\Gamma(q_F^2 + 1)}{2q_F}, \quad (\text{C4})$$

$$\epsilon_{\text{mid}} - \epsilon_0 = \frac{q_F^2 + 1}{q_F + 1},$$

$$\Delta_0 = E_{\text{mid}} - E_0 = \frac{\Gamma(q_F^2 + 1)}{2(q_F + 1)} = \frac{q_F \Delta_m}{q_F + 1},$$

where  $E_{\text{mid}}$  is the energy such that  $T(E_{\text{mid}}) = T(E_{\text{max}})/2$ , which is situated between the minimum at  $E_0$  and maximum at  $E_{\text{max}}$ . In the last line, we have used the relation between  $\Delta_m$  and  $\Gamma$ , given by Eq. (C4). Thus, we may find the parameter  $q_F$  from the energy differences that we know from the experimental curve

$$q_F = \frac{\Delta_0}{\Delta_m - \Delta_0} = \frac{E_{\text{mid}} - E_0}{E_{\text{max}} - E_{\text{mid}}}, \quad (\text{C5})$$

which allows us to obtain the imaginary part of the pole position from Eq. (C4)

$$\Gamma = \frac{2q_F \Delta_m}{q_F^2 + 1}, \quad (\text{C6})$$

and the real part

$$E_p = E_0 + \frac{q_F \Gamma}{2}. \quad (\text{C7})$$

### Appendix D: Time delay

Here we give the explicit formulas for the  $\eta_r$  that are valid in the energy range  $0 < E < K^2/2$ . In the Eq. (30), we denote

$$\begin{aligned} \varepsilon &\equiv \zeta_K + \kappa, \\ \varepsilon_0 &\equiv \Omega^2 \kappa \theta_2, \\ \varepsilon_p &\equiv \varepsilon_0 + \frac{2\Omega^2 \kappa^2}{k^2 + \kappa^2}, \\ \gamma/2 &\equiv \frac{2\Omega^2 \kappa k}{k^2 + \kappa^2}. \end{aligned}$$

Then the resonance part of the scattering phase  $\eta_r$ , Eq. (41), takes the form

$$\eta_r = -\arctan \frac{\gamma}{2(\varepsilon - \varepsilon_p)}.$$

Its energy derivative is

$$\dot{\eta}_r = -\frac{\dot{\gamma}(\varepsilon - \varepsilon_p) - \gamma(\dot{\varepsilon} - \dot{\varepsilon}_p)}{2[(\varepsilon - \varepsilon_p)^2 + (\gamma/2)^2]},$$

where

$$\begin{aligned}\dot{\epsilon} &= \frac{\kappa}{\sqrt{K^2 - k^2}}, \\ \dot{\epsilon}_p &= \Omega^2 \kappa \dot{\theta}_2 - \frac{4\Omega^2 \kappa^2}{(\kappa^2 + k^2)^2}, \\ \dot{\gamma} &= \frac{4\Omega^2 \kappa (\kappa^2 - k^2)}{k(\kappa^2 + k^2)^2}, \\ \dot{\theta}_2 &\approx -\frac{1}{\sqrt{4K^2 - k^2} (\kappa - \sqrt{4K^2 - k^2})^2}.\end{aligned}$$

In the last line we have used the  $n_0 = 3$  approximation for  $\theta_2$ , see Eq. (B8),

$$\theta_2 \approx \frac{1}{\kappa + \zeta_{2K}} = \frac{1}{\kappa - \sqrt{4K^2 - k^2}}.$$

In the  $n_0 = 4$  approximation, see Eq. (B9), we obtain

$$\begin{aligned}\theta_{2,4} &\approx \frac{1}{\zeta_{2K} + \kappa - \frac{\Omega^2}{\zeta_{3K} + \kappa}}, \\ \dot{\theta}_{2,4} &\approx -\theta_{2,4}^2 \left[ \frac{1}{\sqrt{4K^2 - k^2}} + \frac{\Omega^2}{\sqrt{9K^2 - k^2} (\kappa - \sqrt{9K^2 - k^2})^2} \right].\end{aligned}$$

### Appendix E: Bound states

For two wires, for  $\Omega = 0$  the motion along  $\hat{y}$  is described by a 1D Hamiltonian

$$\hat{H}_{y,2} = \frac{\hat{p}_y^2}{2} - \kappa \left[ \delta\left(y - \frac{a}{2}\right) + \delta\left(y + \frac{a}{2}\right) \right] \quad (\text{E1})$$

The bound states, having energy  $E_B^p < 0$  are easily found from the Lippmann-Schwinger equation

$$\begin{aligned}\varphi_b(y) &= -\kappa \int dy' G_{1D}(y - y'; E_B^p) \times \\ &\times \left[ \delta\left(y' - \frac{a}{2}\right) + \delta\left(y' + \frac{a}{2}\right) \right] \varphi_b(y'),\end{aligned} \quad (\text{E2})$$

where  $G_{1D}(y - y'; E)$  is the free-electron Green's function in 1D [37], Eq. (10). Equations (E2) can be solved separately for even and odd functions. After integration and substitution of the expression (10) for the Green's function, Eq. (E2) reduces to

$$\varphi_B^p(y) = \frac{\kappa}{\kappa^p} \left[ e^{-\kappa^p |y - a/2|} + p e^{-\kappa^p |y + a/2|} \right] \varphi_B^p\left(\frac{a}{2}\right), \quad (\text{E3})$$

where  $\kappa^p = \sqrt{2|E_B^p|}$ . From Eq. (E3) we obtain for  $y = a/2$

$$\kappa^p = \kappa \left( 1 + p e^{-\kappa^p a} \right) \quad (\text{E4})$$

$$\approx \kappa \left( 1 + p e^{-\kappa a} \right). \quad (\text{E5})$$

The last approximate equality holds for  $\exp(-\kappa a) \ll 1$ , i.e., in the tight-binding regime. Generally, Eq. (E4) should be solved numerically. The solution is visualized in Fig. 5. We see that the solution for the even bound state  $p = +$  exists for all values of the potential strength  $\kappa$  and the interwire distance  $a$ , whereas the odd bound states,  $p = -$ , exist only for sufficiently large values of the product  $\kappa a > 1$ . Then, in terms of  $\kappa^p$  the binding energy is

$$E_B^p = -\frac{(\kappa^p)^2}{2}.$$

- 
- [1] T. Giamarchi, *Quantum Physics in One Dimension* (Oxford University Press, 2003).
- [2] T. L. Phaedon Avouris, Tony F. Heinz, ed., *2D Materials: Properties and Devices* (Cambridge University Press, Cambridge, 2017).
- [3] L. V. Mario Rocca, Talat S. Rahman, ed., *Springer Handbook of Surface Science*, Springer Handbooks (Springer Cham, Berlin, Heidelberg, 2020).
- [4] V. U. Nazarov, E. E. Krasovskii, and V. M. Silkin, Scattering resonances in two-dimensional crystals with application to graphene, *Phys. Rev. B* **87**, 041405 (2013).
- [5] C. W. Hsu, B. Zhen, A. D. Stone, J. D. Joannopoulos, and M. Soljačić, Bound states in the continuum, *Nature Reviews Materials* **1**, 16048 (2016).
- [6] J. von Neumann and E. P. Wigner, Über merkwürdige diskrete eigenwerte, in *The Collected Works of Eugene Paul Wigner: Part A: The Scientific Papers*, edited by A. S. Wightman (Springer Berlin Heidelberg, Berlin, Heidelberg, 1993) pp. 291–293.
- [7] F. H. Stillinger and D. R. Herrick, Bound states in the continuum, *Phys. Rev. A* **11**, 446 (1975).
- [8] D. R. Herrick, Construction of bound states in the continuum for epitaxial heterostructure superlattices, *Physica B+C* **85**, 44 (1976).
- [9] F. Stillinger, Potentials supporting positive-energy eigenstates and their application to semiconductor heterostructures, *Physica B+C* **85**, 270 (1976).
- [10] L. Fonda and R. G. Newton, Theory of resonance reactions, *Annals of Physics* **10**, 490 (1960).
- [11] H. Friedrich and D. Wintgen, Physical realization of bound states in the continuum, *Phys. Rev. A* **31**, 3964 (1985).
- [12] H. Friedrich and D. Wintgen, Interfering resonances and bound states in the continuum, *Phys. Rev. A* **32**, 3231 (1985).
- [13] M. Pizarra, P. Riccardi, A. Sindona, A. Cupolillo, N. Ligato, C. Giallombardo, and L. Caputi, Probing graphene interfaces with secondary electrons, *Carbon* **77**, 796 (2014).
- [14] F. Wicki, J.-N. Longchamp, T. Latychevskaia, C. Escher, and H.-W. Fink, Mapping unoccupied electronic states of freestanding graphene by angle-resolved low-energy elec-

- tron transmission, *Phys. Rev. B* **94**, 075424 (2016).
- [15] M. Krivenkov, D. Marchenko, J. SÁnchez-Barriga, O. Rader, and A. Varykhalov, Suppression of electron scattering resonances in graphene by quantum dots, *Applied Physics Letters* **111**, 161605 (2017).
- [16] B. Matta, P. Rosenzweig, O. Bolkenbaas, K. Küster, and U. Starke, Momentum microscopy of Pb-intercalated graphene on SiC: Charge neutrality and electronic structure of interfacial Pb, *Phys. Rev. Res.* **4**, 023250 (2022).
- [17] T. A. de Jong, J. Jobst, H. Yoo, E. E. Krasovskii, P. Kim, and S. J. van der Molen, Measuring the Local Twist Angle and Layer Arrangement in Van der Waals Heterostructures, *physica status solidi (b)* **255**, 1800191 (2018).
- [18] B. Da, Y. Sun, Z. Hou, J. Liu, N. T. Cuong, K. Tsukagoshi, H. Yoshikawa, S. Tanuma, J. Hu, Z. Gao, and Z. Ding, Measurement of the low-energy electron inelastic mean free path in monolayer graphene, *Phys. Rev. Appl.* **13**, 044055 (2020).
- [19] P. S. Neu, D. Geelen, A. Thete, R. M. Tromp, and S. J. van der Molen, Complementary LEEM and eV-TEM for imaging and spectroscopy, *Ultramicroscopy* **222**, 113199 (2021).
- [20] M. Ewert, L. Buß, N. Braud, A. K. Kundu, P. M. Sheverdyeva, P. Moras, F. Genuzio, T. O. Mentes, A. Locatelli, J. Falta, and J. I. Flege, The Transition from MoS<sub>2</sub> Single-Layer to Bilayer Growth on the Au(111) Surface, *Frontiers in Physics* **9**, 10.3389/fphy.2021.654845 (2021).
- [21] C. Hong, W. Zou, P. Ran, K. Tanaka, M. Matzelle, W.-C. Chiu, R. S. Markiewicz, B. Barbiellini, C. Zheng, S. Li, A. Bansil, and R.-H. He, Anomalous intense coherent secondary photoemission from a perovskite oxide, *Nature* **617**, 493 (2023).
- [22] M. Corso, J. Lobo-Checa, A. P. Weber, I. Piquero-Zulaica, Z. M. A. El-Fattah, P. L. Fèvre, J. E. Ortega, and E. Krasovskii, Enhanced vacuum ultraviolet photoemission from graphene nanoribbons, *2D Materials* **11**, 015008 (2023).
- [23] E. Kogan, V. U. Nazarov, V. M. Silkin, and M. Kaveh, Energy bands in graphene: Comparison between the tight-binding model and ab initio calculations, *Phys. Rev. B* **89**, 165430 (2014).
- [24] E. Kogan and V. M. Silkin, Electronic structure of graphene: (Nearly) free electron bands versus tight-binding bands, *physica status solidi (b)* **254**, 1700035 (2017).
- [25] Y. Ueda, Y. Suzuki, and K. Watanabe, Time-dependent first-principles study of angle-resolved secondary electron emission from atomic sheets, *Phys. Rev. B* **97**, 075406 (2018).
- [26] T. P. Grozdanov and E. A. Solov'ev, 3D scattering by 2D periodic zero-range potentials: total reflection/transmission and threshold effects, *The European Physical Journal B* **95**, 16 (2022).
- [27] T. P. Grozdanov and E. A. Solov'ev, Canal states in bilayer thin films of zero-range potentials, *The European Physical Journal Plus* **139**, 425 (2024).
- [28] U. Fano, Effects of configuration interaction on intensities and phase shifts, *Phys. Rev.* **124**, 1866 (1961).
- [29] C. Ott, A. Kaldun, L. Argenti, P. Raith, K. Meyer, M. Laux, Y. Zhang, A. Blättermann, S. Hagstotz, T. Ding, R. Heck, J. Madroñero, F. Martín, and T. Pfeifer, Reconstruction and control of a time-dependent two-electron wave packet, *Nature* **516**, 374 (2014).
- [30] P. C. Deshmukh, A. Kumar, H. R. Varma, S. Banerjee, S. T. Manson, V. K. Dolmatov, and A. S. Kheifets, Wigner–eisenbud–smith photoionization time delay due to autoionization resonances, *Journal of Physics B: Atomic, Molecular and Optical Physics* **51**, 065008 (2018).
- [31] S. Banerjee, P. C. Deshmukh, V. K. Dolmatov, S. T. Manson, and A. S. Kheifets, Strong dependence of photoionization time delay on energy and angle in the neighborhood of Fano resonances, *Phys. Rev. A* **99**, 013416 (2019).
- [32] P. C. Deshmukh, S. Banerjee, A. Mandal, and S. T. Manson, Eisenbud–Wigner–Smith time delay in atom–laser interactions, *The European Physical Journal Special Topics* **230**, 4151 (2021).
- [33] D. Bohm, *Quantum Theory* (Prentice-Hall, New York, 1951).
- [34] E. P. Wigner, Lower limit for the energy derivative of the scattering phase shift, *Phys. Rev.* **98**, 145 (1955).
- [35] F. T. Smith, Lifetime matrix in collision theory, *Phys. Rev.* **118**, 349 (1960).
- [36] E. E. Krasovskii and R. O. Kuzian, Negative transit time in non-tunneling electron transmission through graphene multilayers (2024), arXiv:2404.19440 [cond-mat.mtrl-sci].
- [37] E. Economou, *Green's Functions in Quantum Physics* (Springer-Verlag, Berlin, Heidelberg, 2006).
- [38] R. Haydock, The Recursive Solution of the Schrödinger Equation, in *Solid State Physics*, Vol. 35, edited by H. Ehrenreich, F. Seitz, and D. Turnbull (Academic Press, 1980) pp. 215–294.
- [39] V. S. Viswanath and G. M. Müller, Hamiltonian representation, in *The Recursion Method: Application to Many-Body Dynamics* (Springer Berlin Heidelberg, Berlin, Heidelberg, 1994) pp. 32–50.
- [40] L. Landau and E. Lifshitz, *Quantum Mechanics: Non-Relativistic Theory*, Course of theoretical physics (Elsevier Science, 1981).
- [41] W. J. Lentz, Generating Bessel functions in Mie scattering calculations using continued fractions, *Appl. Opt.* **15**, 668 (1976).
- [42] I. Thompson and A. Barnett, Coulomb and Bessel functions of complex arguments and order, *Journal of Computational Physics* **64**, 490 (1986).
- [43] W. H. Press, S. A. Teukolsky, W. T. Vetterling, and B. P. Flannery, *Numerical Recipes 3rd Edition: The Art of Scientific Computing*, 3rd ed. (Cambridge University Press, USA, 2007).